Effect of Thermal Motions on the Structure and UV−Visible Electronic Spectra of Stilbene and Model Oligomers of Poly(*p*-Phenylene Vinylene)

S. P. Kwasniewski, J. P. François, and M. S. Deleuze*

Limburgs Universitair Centrum, Instituut voor Materiaal Onderzoek, Departement SBG, Universitaire Campus, Gebouw D, B-3590 Diepenbeek, Belgium

Received: August 9, 2002; In Final Form: February 4, 2003

In the present study, we investigate the influence of temperature on the width and location of bands in the UV−visible absorption spectra of oligomer chains of poly(*p*-phenylene vinylene) (PPV). These spectra have been computed by means of molecular dynamics (MD) simulations along with the classical MM3 force field, in conjunction with (Z)INDO/S-CIS calculations of vertical excitation energies and transition moments. In addition, the MD(MM3) computations enable consistent insights into the average structures of *cis*- and *trans*-stilbene, at temperatures ranging from 0 to 500 K. For *trans*-stilbene and larger PV-*n* oligomer chains converging to PPV, thermal motions at room temperature in the vacuum result in a constant broadening of bands by 24 nm (0.20 eV) at half the maximum. Compared with the trans-isomer, thermal broadening intensifies to 33 nm (0.44 eV) for *cis*-stilbene, due to enhanced steric effects. When accounting in addition for the outcome of vibronic broadening, the width of the first absorption band increases at 300 K to 33 nm (0.48 eV) for *trans*-stilbene and ∼46 nm (0.40 eV) for the largest PV-*n* chains. At last, upon studying a large molecular cluster reproducing the crystalline structure of *trans*-stilbene, it has been found that, although they strongly impede the rotations of phenyl rings and out-of-plane distortions, packing effects and steric hindrances in the solid phase lead to a limitation of the width of the first absorption band by 6 nm (0.07 eV) only at 300 K.

Introduction

The discovery of the electrical conductivity of doped polyacetylene[1] has triggered a revolution in the perception of polymer materials. Low-band gap oligomers and polymers are nowadays a major research topic (see, e.g., refs 2−4), with useful technological applications materializing in many areas. The genuine interest in these polymers stems from the fact that they combine the optical and electronic properties of semiconductors, together with the lightness and engineering facilities of plastics,[5] a major advantage for numerous applications in microelectronics. Unsurprisingly, therefore, conjugated polymers are nowadays key components of a number of advanced but rather low-cost electronic devices, such as light-emitting diodes (LED's),[6] electrochromic displays and windows,[7] field effect transistors,[8,9] anti-static layers,[10] solar cells,[11] sensors,[12] and solid or gel cell lithium batteries.[13]

Among these low band gap compounds, one of the most intensively studied conjugated polymers is poly(*p*-phenylene vinylene) (PPV), an intrinsically electroluminescent polymer (see, e.g., ref 14). One of its "tuned" derivatives, known as OC_1C_{10}, has recently been exploited in commercial devices such as polymer LED's.[15] This structure carries a methyl and a longer alkyl chain coupled to each of the phenyl rings through an ether function, which keep chains at larger distances because of intermolecular steric hindrances, and thereby limit the quenching resulting from interchain hopping of charges. *trans*-stilbene is the smallest molecule that reproduces the basic electronic and geometric structure of PPV (Figure 1a). The low-lying electronically excited states of this molecule have been extensively investigated using a variety of advanced ab initio methods (see, e.g., refs 16−18). One of the strongest motivations for carrying out such studies relates to the photoisomerization of this

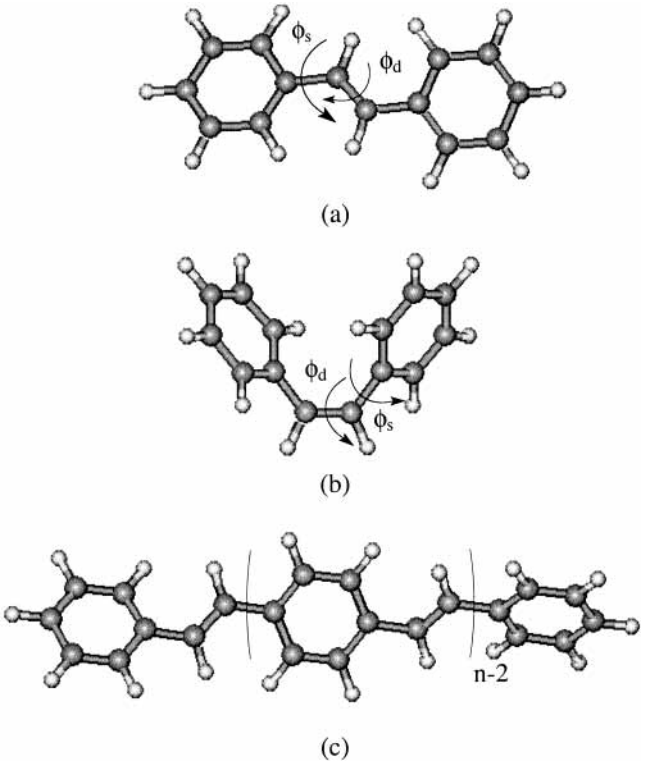

Figure 1. (a) Structure of *trans*-stilbene. ϕ_s and ϕ_d are the torsion angles around the vinylene single and double bonds, respectively. (b) Structure of *cis*-stilbene. (c) Structure of the PV-*n* oligomers (with *n* the number of phenyl rings).

* Corresponding author. E-mail: deleuze@luc.ac.be.

10.1021/jp021853b CCC: $25.00
Published on Web 06/07/2003

molecule (see, e.g., refs 19 and 20), a process of utmost importance in e.g. biological reactions.

Despite so many theoretical and experimental studies on the electronic absorption spectra of the PPV polymer and of related oligomers, the problem of band broadening remains at present a largely unresolved issue. As is well-known, the spectral line relating to a given electronically excited state is in practice broadened due to numerous effects, such as natural line broadening, the Doppler effect, intermolecular collisions, instrumental broadening, environment effects, vibronic coupling, and thermal motions (see, e.g., ref 21). One study of relevance for the present contribution is an experimental determination of the outcome of matrix and temperature effects, as well as vibronic couplings, on optical spectra of PPV derivatives.[22]

For conjugated polymers such as PPV, several additional factors can be retained that further contribute to band broadening. The extent of straight planar chain segments shows most commonly a broad distribution, due to the inherent structural disorder of polymer matrixes. Because this extent determines the effective conjugation length in the PPV polymer (see, e.g., refs 23 and 24), strong distortions from planarity as well as sp^3 defects could provide a first explanation of the particularly strong and inhomogeneous band broadening (150 nm or more) seen in the available absorption spectra of PPV.[25] These conjugated segments determine the spatial extent of the electronic wave function, which in turn controls the Franck−Condon overlap integrals determining the intensities of lines in the vibronic progressions. As such, the average conjugation length and the extent of geometric relaxation in the excited states can be estimated from measurements.[26,27] From a comparison of absorption spectra of PPV with the spectra of a series of finite PV-*n* oligomers (with *n* the number of phenyl rings in the system), it has been conjectured that the largest conjugation lengths range from 10 to 20 monomer units (see, e.g., refs 28 and 29). π-delocalization in conjugated polymers is limited not only by structural disorder, but also by temperature-induced excitation of vibrational, rotational, or librational motions (see, e.g., refs 30−32). Furthermore, in a polymer matrix, interchain interactions through overlap of the individual electronic wave functions can lead to a splitting of electronic states, referred to as a Davydov splitting. This splitting, which is not considered in this work, induces a blue shift of the lowest optically allowed transition in a cofacial configuration with respect to the isolated molecule.[33] In the most ideal cases, e.g., a cofacial configuration, Davydov splittings up to 0.3 eV have been reported from (Z)-INDO/S-CIS calculations on *trans*-stilbene molecules at an interchain distance of 4 Å.[33] Another possible source of broadening, which is also dropped from the present study, concerns the average distribution of trans- and cis-isomers (see, e.g., ref 34).

Clearly, despite the impressive growth of computer power and software developments, a complete description of all the components affecting the electronic spectrum of a polymer within one single theoretical model remains a highly elusive target. In the present study, we will provide one piece to this puzzling and complicated issue, by studying at different temperatures the impact of thermal motions on the position and shape of pure electronic absorption bands. It should be stressed that none of the theoretical studies so far of the electrooptical properties of conducting polymers have ever explicitly tackled the outcome of thermal dynamic disorder. Most commonly, the effect of temperature is simply accounted for in the simulations through convolutions using an appropriate (Gaussian, Lorentzian, or Voigt) spread function with a fwhm (full width at half-maximum) parameter of 20 nm at room temperature. Notice that even with spectral measurements on PPV oligomers at 80 K, a spread function with a fwhm of 10 nm is necessary to ensure consistent insights from the simulations (see, e.g., ref 35). As shall be shown, this broadening is fully consistent with the outcome of thermal motions of PPV oligomers in the gas phase. In the present study, conclusions for the polymer are drawn from extrapolations of calculations on a series of finite model molecular chains converging to PPV. The calculations are based on molecular dynamics (MD) simulations along with a classical molecular mechanics (MM) force field, followed by (Z)INDO/S-CIS computations of vertical electronic transitions on structures extracted from the MD simulations.

In addition, this investigation also compares both the thermally averaged structure and optical bands of a crystalline cluster of *trans*-stilbene molecules with that of isolated molecules. In a crystal, large-amplitude motions are expected to be impeded by the steric hindrances with the surrounding molecules. However, an unusually short length (1.338 Å) has been reported for the central vinylene C═C bond in recent X-ray diffraction studies of *trans*-stilbene.[36] These studies give evidence that complete and synchronous rotations of the phenyl rings about the single C−C bond are still possible in a crystal matrix, in the form of a pedaling motion, described by a 2-fold rotation of the central ethylene bond about the longitudinal axis of the molecule.[37−39] The occurrence of such large-amplitude motions motivates further the present investigation of the impact of dynamic disorder on the electronic properties of *trans*-stilbene and related compounds.

Methodological Considerations and Justifications

Molecular mechanics (MM)[40] and molecular dynamics (MD)[41] are used to study, among others, the structure of macromolecules, disorder effects in crystalline structures, and solvent interactions.[42−45] In the present study, Allinger's classical MM3 force field[46−48] has been selected for performing the MD computations, because with this force field the stretching, bending, and torsion force constants in conjugated segments can be refined at all steps of the calculations through iterative SCF calculations of the π-density.[49,50] As such, this force field affords consistent insights into the out-of-plane deformations of aromatic rings. It is also well suited for obtaining molecular structures and evaluating conformational energies and rotational barriers in strained (cyclic and cage) hydrocarbon structures and aromatic compounds (see, e.g., refs 51−53). In particular, for *trans*-stilbene, MM3 has been shown in a preliminary study[54] to enable a consistent treatment of the out-of-plane rotation of the phenyl rings up to a value of 60°, compared with DFT-B3LYP/cc-pVDZ calculations including the leading effects of electron correlation. Also, the MM3 force field enables a quantitative determination of the crystalline architecture of PV-8 oligomers,[42] both for the molecular structures and lattice parameters. Also of relevance for the present work is a detailed MM3 study of the pedaling motions of *trans*-stilbene within the field of a mean crystal lattice, which has led to a quantitative description of the anomalous temperature dependence of the central vinylene bond length.[55] At the very last, the MM3 force field has been shown to surpass in accuracy B3LYP/cc-pVDZ calculations of the single-bond rotational barriers of *trans*-stilbene, in comparison with benchmark quantum-mechanical results derived from a focal point analysis.[56] At last, this force field affords consistent insights into complex molecular motions, such as the circumrotations of benzylic amide catenanes,[57] and the spinning of C_{60} cages in the solid phase.[58]

The MD(MM3) computations have been performed using the 3.1 version of the TINKER package of programs.[59] Atom types "2" and "5" have been used for all sp^2-carbon and hydrogen atoms, respectively. Different temperatures have been imposed in these simulations through coupling of the system with an external bath using the Groningen method.[60] The trajectories are calculated using the modified Beeman algorithm,[61] along with the following inputs for the MD computations: an integration time step of 0.25 fs, a thermal equilibration time of 0.01 ns, a dump time of 0.1 ps, and a total run time of 0.11−0.36 ns. The outcome of accumulated deviations in the MD-(MM3) computations, arising as numerical instabilities due to a possibly too limited integration step, or of a too limited exploration of the phase space by the MD trajectories have been carefully assessed for *trans*-stilbene, by comparison with the results derived from MD runs using different input parameters.[54] With the set of parameters selected here, it has been found in particular that the impact of the highest-frequency molecular motions, associated with the C−H bonds, on the width of the first absorption band, is less than 0.05 nm (0.004 eV) at room temperature.[54] The potential and total energies of the configurations produced by the MD runs have been carefully monitored, to ensure a consistent exploration of phase space. It has been observed that the equilibration time required to ensure stabilization of the energy of the system within 10% of its thermally averaged value is less than 2 ps and decreases with increasing system size. An equilibration time of 0.01 ns has been systematically used throughout this study, which is largely sufficient to ensure a consistent thermalization.

The results of the MD(MM3) simulations are analyzed to evaluate the effect of thermal agitation on the conformational properties of oligomers of PPV in the gas phase. In particular, attention has been focused on four geometrical parameters, with regard to their leading influence on the absorption spectrum of *trans*-stilbene, as already pointed out in ref 54. The determination of the thermally averaged values for the bond lengths of the central vinylene single and double bonds, and for the dihedral angle describing the torsion of the central vinylene double bond, ϕ_d (Figure 1), is straightforward. On the other hand, when estimating the average torsion of the vinylene single bonds, ϕ_s (Figure 1), from the MD outputs, some care is needed to make consistent comparisons with experiments. First, the reported experimental data (see, e.g., ref 62) were obtained from experiments that cannot discriminate structures with opposite enantiomeric character (hence experimental values are actually reported as $\bar{\phi}_s = \langle \phi_s^2 \rangle^{1/2}$). Thus, to evaluate the average out-of-plane distortion of stilbene at different temperatures, the average of the absolute values of ϕ_s has to be considered. Second, at sufficiently high temperatures ($T \geq 400$ K), another difficulty arises: both for *trans*- and *cis*-stilbene, the rotational barrier at $\phi_s = 90°$ can be occasionally exceeded, implying that the two C⋯C bonds, adjacent to the vinylene single bond, are swapped in the studied phenyl ring. This in turn can lead to some ambiguity in the assignment of ϕ_s. Assuming that the phenyl rings remain planar despite the thermal motions, this ambiguity can be released as follows:

Case I: The absolute values of ϕ_s comprised between 0 and 90° are accounted for as such.

Case II: The absolute values of ϕ_s comprised between 90 and 180° are subtracted from 180°.

In a further step, (Z)INDO/S-CIS[63,64] calculations are performed using the ZINDO package[65] by Zerner upon large sets of structures (typically: 2000−3500 molecular geometries) extracted from the MD(MM3) simulations at different temperatures. Compared with more reliable but much more demanding TD-DFT[66−68] and CASPT2[69] calculations, it has been found that the (Z)INDO/S-CIS scheme by Zerner[70] enables calculations of the low-lying valence excited states of *trans*-stilbene with an accuracy of 0.2 eV on the computed one-electron excitation energies.[18] The reliability of this semiempirical scheme has been amply assessed through comparison against experimental data for polymers (see, e.g., refs 71 and 72). In the present work, the accuracy of the (Z)INDO/S-CIS approach in describing the excitation spectra of nonequilibrium, distorted structures has been further verified by comparison with TD-DFT computations, in conjunction with the B3LYP functional and the cc-pVDZ basis set, on structures optimized at the B3LYP/cc-pVDZ level under the constraint of a C_2 symmetry point group and of fixed torsion angles ϕ_s with values ranging from 0 to 90° (see Table 1). Upon examining this table, it is immediately apparent that the first absorption line is predicted within 0.1 eV accuracy up to torsion angles ϕ_s of 40°. More specifically, at the (Z)INDO/S-CIS level, compared with the TD-B3LYP/cc-pVDZ one, the wavelengths associated with the first excitation energies are systematically overestimated by ∼7.3 nm, whereas the corresponding oscillator strengths are systematically underestimated by ∼0.2 au. Also, the five lowest-lying vertical (Z)-INDO/S-CIS excitation energies do not deviate by more than 0.2 eV from the TD-B3LYP/cc-pVDZ results, up to (double) torsions ϕ_s of 60°. The agreement deteriorates for larger synchronous rotations of both phenyl rings about the single carbon−carbon bonds (0.3 and 1.2 eV disagreements are for instance noticed for the first excitation energy, for structures of C_2 symmetry characterized by torsion angles ϕ_s equal to 60° and 90°, respectively). Notice, however, that these strongly and doubly twisted conformations are 5.7 and 12.0 kcal mol^{-1} less stable than the planar (C_{2h}) structure, and are therefore thermostatistically very unsignificant.

A first series of (Z)INDO/S-CIS calculations of UV−visible absorption spectra at specific temperatures for *trans*- and *cis*-stilbene and PV-*n* ($n = 2-4$) has been carried out without any restrictions of the orbital active space, except for the frozen core approximation. To make computations possible on larger systems, a second series of calculations for oligomers up to PV-7 has been performed with the valence active space restricted to π-orbitals only. It has been found that this restriction of active space results in a nearly constant blue shift of the wavelength describing the first absorption line (hereafter λ_{max}) by 26.2 nm (Figure 2a). Correspondingly, the related oscillator strength is increased by a value (Figure 2b), which, upon fitting, scales on average as

$$\Delta F = 0.1264 \ln(n) + 0.1253 \qquad (1)$$

with a (R^2) correlation coefficient of 0.9926. In the sequel of this study, the absorption thresholds of the species PV-5, PV-6, and PV-7 have therefore been corrected by a red shift of 26.2 nm, and the corresponding oscillator strengths have been rescaled according to $F' = F - \Delta F$. Notice that the restriction of the active space no longer allows a consistent description of the remaining B and C absorption bands, due to the neglect of the configurational mixing with the σ and σ^* levels. Therefore, these bands have been dropped from the simulations for PV-*n* chains larger than PV-4.

The influence of dynamic disorder within the field of a crystal lattice has also been investigated at room temperature on similar grounds for *trans*-stilbene. For this purpose, molecular structures have been extracted from MD(MM3) computations on a model crystalline cluster of 58 molecules, characterized by a radius of

TABLE 1: Vertical Energies (E) and Oscillator Strengths (F) of *trans*-Stilbene

	TD-B3LYP[a]			INDO/S-CIS			
planar	*E* (nm)	*E* (eV)	*F*	*E* (nm)	*E* (eV)	*F*	B3LYP[a,b] E_{rel} (kcal mol^{-1})
				2 × 0°			
$1B_u$	314.7	3.94	0.968	322.0	3.85	1.108	0.0 (0.0)
$2B_u$	273.1	4.54	0.010	286.3	4.33	0.011	
$3B_u$	240.6	5.15	0.175	225.4	5.50	0.547	
$4B_u$	196.5	6.31	0.063	221.0	5.61	0.731	
$5B_u$	195.2	6.35	0.005	201.9	6.14	0.467	
				2 × 10°			
1B	313.1	3.96	0.958	320.2	3.87	1.095	0.1 (0.0)
2B	272.5	4.55	0.010	285.7	4.34	0.011	
3B	240.2	5.16	0.164	224.9	5.51	0.514	
4B	198.5	6.25	0.020	221.0	5.61	0.741	
5B	197.3	6.28	0.047	209.9	5.91	0.018	
6B	195.6	6.34	0.005	201.8	6.14	0.441	
				2 × 20°			
1B	308.2	4.02	0.935	315.4	3.93	1.069	0.4 (0.2)
2B	270.1	4.59	0.008	284.7	4.35	0.012	
3B	238.9	5.19	0.133	224.7	5.52	0.403	
4B	199.3	6.22	0.024	221.0	5.61	0.758	
5B	198.9	6.23	0.028	209.7	5.91	0.078	
6B	196.5	6.31	0.002	202.2	6.13	0.362	
				2 × 30°			
1B	299.7	4.14	0.900	307.2	4.04	1.028	1.0 (0.8)
2B	266.1	4.66	0.006	282.9	4.38	0.012	
3B	236.4	5.25	0.093	224.3	5.53	0.307	
4B	200.9	6.17	0.012	220.4	5.63	0.726	
5B	200.5	6.18	0.032	209.5	5.92	0.181	
6B	197.0	6.29	0.0004	202.2	6.13	0.234	
				2 × 40°			
1B	287.7	4.31	0.843	295.7	4.19	0.971	2.2 (1.8)
2B	260.3	4.76	0.003	280.5	4.42	0.012	
3B	232.6	5.33	0.056	224.1	5.53	0.315	
4B	203.2	6.10	0.011	218.7	5.67	0.586	
5B	202.2	6.13	0.023	209.3	5.92	0.245	
6B	197.3	6.29	0.0006	201.9	6.14	0.107	
				2 × 60°			
1B	258.3	4.80	0.609	275.1	4.51	0.006	5.7 (5.0)
2B	246.0	5.04	0.001	268.4	4.62	0.792	
3B	222.5	5.57	0.030	224.7	5.52	0.418	
4B	207.9	5.96	0.006	213.5	5.81	0.267	
5B	205.3	6.04	0.008	210.9	5.88	0.173	
				S2 (2 × 90°)[c]			
$1A_u$	227.7	5.45	0.001	266.2	4.66	0.011	9.4 (7.3)
$2A_u$	207.4	5.98	0.004	214.3	5.79	0.060	
$1B_u$	205.5	6.03	0.0001	236.0	5.25	0.166	
$3A_u$	204.8	6.05	0	200.9	6.17	1.373	
$2B_u$	202.1	6.14	0.044	211.5	5.86	1.879	
$3B_u$	201.4	6.16	0.001	197.6	6.27	0.109	

[a] cc-pVDZ basis set. [b] Values in brackets are MM3 relative energies. [c] Ref 56.

about 20 Å. The initial crystalline structure was built according to the results of a X-ray diffraction study at −160 °C[62] (Figure 3). The monoclinic space group of the crystal is $P2_1/a$, and the cell dimensions are $a = 12.287$, $b = 5.660$, $c = 15.478$ Å, and $\beta = 112.03°$. The cells contain two-half, independent molecules, denoted as α and β, in the asymmetric unit, which lies at two nonequivalent inversion centers in the unit cell, and are very nearly related by a 2-fold screw axis parallel to the *c* axis. The molecular structure of these two molecules differ slightly (e.g., ϕ_s values of 3.4° and 6.9° are reported for the α and β-molecules, respectively[62]). To roughly mimic the "crystal pressure", the "sphere" keyword of the TINKER package of programs was used to inactivate all atoms positioned at a distance of more than 15 Å from the center of the cluster. A total of 24 molecules are fully enclosed within this sphere. The

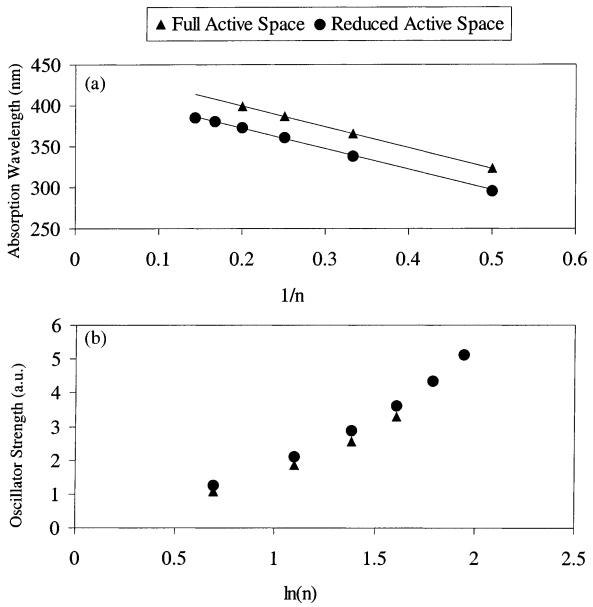

Figure 2. Size dependence of (a) λ_{max} (linear regressions given by $y_f = -254.22\ 1/n + 449.41$ and $y_r = -249.48\ 1/n + 421.37$, where f and r refer to (Z)INDO/S-CIS//MM3 calculations with a complete active space, or with an active space restricted to π-π^* excitations only. (b) Corresponding oscillator strengths (*n* denotes the number of phenyl rings in the oligomer).

π-electron SCF computations involved in the MM3 calculations make large scale MD simulations on such clusters completely untractable. To overcome this difficulty, the MM3 force field constants, obtained from the π-SCF computations on a single *trans*-stilbene molecule, are retained for all 58 molecules in the cluster, neglecting thereby the impact that intermolecular motions and distortions of the molecular structure may have on the electron densities. At first glance, this may seem a rather drastic approximation. However, upon verification from further combined (Z)INDO/S-CIS//MD(MM3) calculations of the gas-phase absorption spectra of *trans*-stilbene at room temperature, it appears that freezing the π-electron densities and the related force constants to the 0 K values has a very negligible impact (less than 2 nm or 0.02 eV, and 1 nm or 0.02 eV, respectively) on the computed bandwidths, and on λ_{max}. Furthermore, it has been found that this simplified force field, denoted as MM3′, does not very significantly deviate from the standard MM3 and B3LYP/cc-pVDZ single-bond torsion potentials about ϕ_s (Figure 4). All three methods (MM3, MM3′, and B3LYP/cc-pVDZ) give consistent insights, within less than 0.5 kcal mol^{-1}, into the rotation of the phenyl rings about the vinylene C−C bonds, up to values of ϕ_s approaching 60°.

Further MM3, MM3′, and B3LYP/cc-pVDZ calculations have been carried out to study in detail the torsion potential of *trans*-stilbene near equilibrium with respect to variations of the double-bond torsional angle ϕ_d. These results are displayed in Figure 5 and demonstrate that the MM3, MM3′, and B3LYP/cc-pVDZ torsion potentials do not deviate by more than 0.5 kcal mol^{-1}, up to $\phi_d = 12°$, which is sufficient to reliably investigate the outcome of thermal motions on this internal coordinate at 300 K (at this temperature, the thermodynamical weight of structures with a torsion angle ϕ_d larger than 12° is less than 10%; see further).

The average results obtained finally for the geometries and electronic properties are, in practice, independent of the sets of selected molecular structures, given they are extracted for a given α or β-molecule in the cluster, or from a mixture of both. The results shown in the sequel for the cluster, modeling the

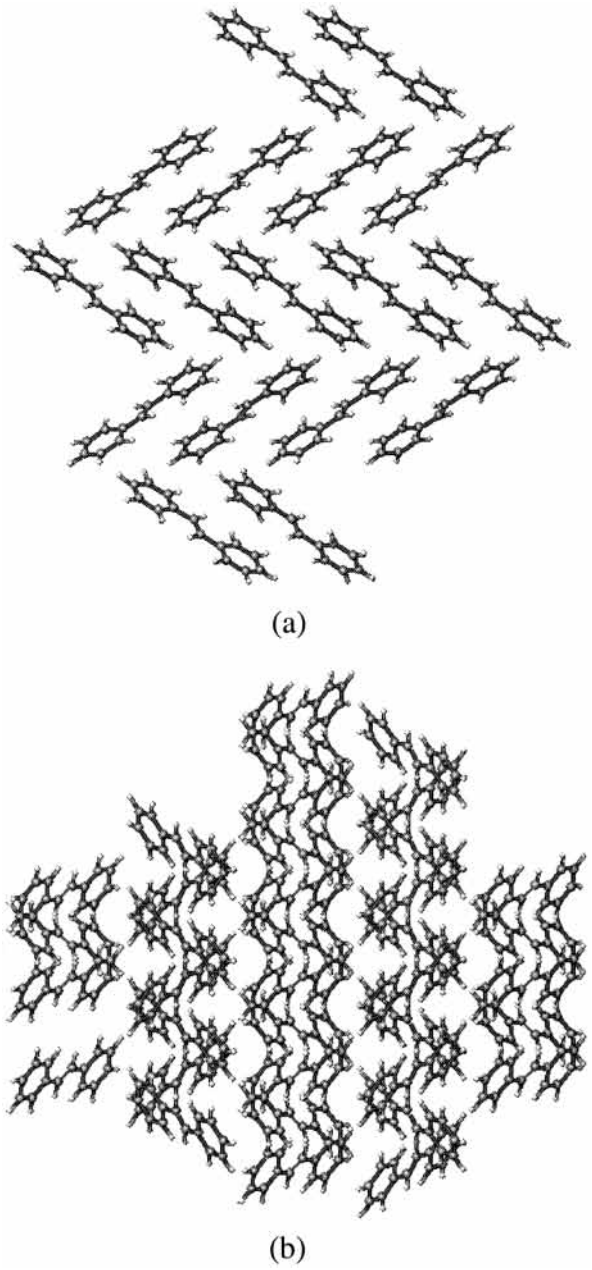

Figure 3. Model crystalline cluster of *trans*-stilbene, based on the data published in ref 61. The crystal structure is shown along (a) the *b* and (b) the *c* axis.

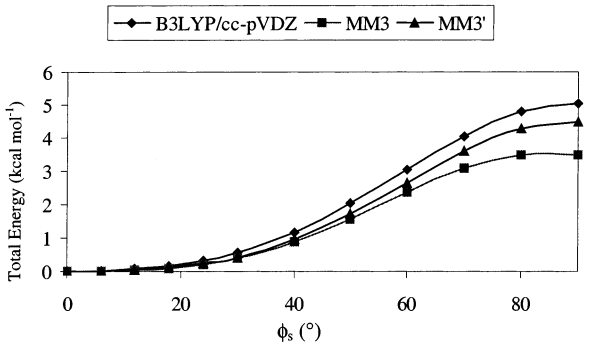

Figure 4. Dependence of the relative energy of *trans*-stilbene on the torsion of a single phenyl ring around the vinylene single bond, at the MM3, MM3′, and B3LYP/cc-pVDZ theoretical levels.

crystalline form of *trans*-stilbene, are the outcome of the thermal motions of a β-stilbene molecule at the center of the sphere

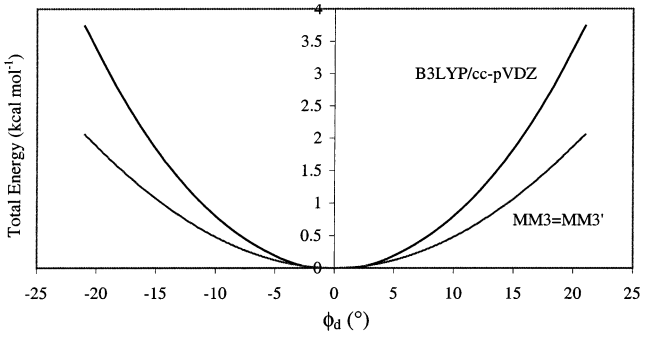

Figure 5. Torsion potential of the central vinylene double bond of trans-stilbene at the MM3, MM3′, and B3LYP/cc-pVDZ levels of theory.

in which molecular motions are permitted. In this case, (Z)INDO/S-CIS calculations are performed within the frozen core approximation on a large set of molecular structures (3000) extracted from the MD(MM3′) simulation on the model crystalline cluster. Notice that these (Z)INDO/S-CIS calculations are carried out on an individual molecular basis, so that the Davydov splitting of lines, due to the overlap of the electronic wave functions, is not accounted for.

To enable easy comparison with experimental spectra, all resulting absorption lines are summed and convoluted using as spread function a linear combination of one Gaussian and one Lorentzian function of equal weight and width. A fwhm of 2 nm (corresponding to 0.025 eV for *trans*-stilbene, or to 0.015 eV for PV-7) is used throughout the present work, to account for the natural and standard instrumental broadenings. The resulting convoluted absorption spectra have been normalized onto the scale of a single molecule, which enables direct comparison of absolute intensities for all simulations. The temperature effect on the first absorption line is analyzed through a description of the resulting band (A) by a Gaussian function, using the linearization method described in ref 54. All broadenings reported in the sequel refer to full bandwidth at half-maximum (fwhm).

Finally, the cumulated effect of thermal and vibronic broadenings has been reevaluated for the first absorption band by means of an elementary theoretical approach based on the harmonic Franck−Condon approximation (see, e.g., ref 73) for calculating vibronic sequences, in conjunction with the (Z)-INDO/S-CIS//MD(MM3) procedure described so far. The purpose of this extension is not to provide quantitative calculations of vibronic sequences, which should require more elaborate treatments,[73] but simply to compare on qualitative grounds the overall relative impact of thermal and vibronic broadenings. Because using only one or two effective vibrational modes makes in practice little difference in the obtained vibronic sequences (see Figure 4 in ref 35), the energies of lines in the vibronic sequences pertaining to the first excited state of each selected PV-*n* structure in the MD(MM3) runs have been calculated using only one effective vibronic mode

$$\epsilon_{0\nu} = \epsilon_{00} + \nu\hbar\omega \qquad \text{with} \qquad \nu = 0, 1, ..., 5 \qquad (2)$$

where ν is the vibrational quantum number and ϵ_{00} and $\epsilon_{0\nu}$ are the vertical one-electron transition energies (in electronvolts) from the zeroth vibrational energy level of the ground-state structure to the zeroth and the νth vibrational quantum levels of the first electronic excited state, respectively. The selected vibrational quantum, ω, amounts to 0.18 eV, an energy that corresponds to the average spacing of lines seen with site-

selective fluorescence spectroscopy for the vibronic progression derived from the first excited (^1B_u) state of *trans*-stilbene.[26,35]

The total spectral intensity, $I(\lambda)$, accounting for both thermal and vibronic broadenings, is then calculated by summing the intensities derived for the related vibronic distributions over all the molecular structures extracted from the MD(MM3) outputs. The latter are calculated on an individual molecular basis, as follows[73]

$$I(\lambda) \cong \frac{F}{\lambda}\sum_{\nu=0}^{5}\frac{(S_\omega)^{\nu_e - S_\omega}}{\nu!}D(\lambda - \lambda_{0\nu}) \qquad (3)$$

with $\lambda_{0\nu}$ the wavelength relating to the $0-\nu$ vibronic transition. The individual intensities in the vibronic sequence are scaled against the oscillator strength F, calculated for the $0-0$ transition. The fraction in the summation over the vibrational quantum levels on the right-hand side of eq 3 is the Franck−Condon factor, characterizing the electronic transition. The fitted Huang−Rhys factors, S_ω, which are formally proportional to the coordinate displacements induced by adiabatic electronic transitions, have been taken from ref 35 (1.95 for *trans*-stilbene and 1.60 for the larger oligomers). The spread function $D(\lambda - \lambda_{0\nu})$ required to convolute the vibronic sequence is again a linear combination of one Gaussian and one Lorentzian function of equal weight and width (fwhm = 2 nm). The intensities of higher-lying vibronic transitions ($\nu > 5$) are negligible, due to the $1/\nu!$ factor, and have therefore been dropped from the present computations.

Results and Discussion

***trans*- and *cis*-Stilbene.** The ground state geometries of *trans*- and *cis*-stilbene are the outcome of a tricky balance between steric and electronic (conjugation) effects. In the case of *trans*-stilbene, steric interactions between the vinylene hydrogen atoms and the adjacent H atoms in the ortho-positions of the phenyl rings are weak and can be easily overcome by conjugation effects, which favor planarity. Therefore, at the MM3 level, a planar C_{2h} structure is found for *trans*-stilbene. This is in agreement with geometry optimizations within a C_2 point group at theoretical levels such as PM3,[74] CASSCF,[16] and DFT/B3LYP,[18,75] leading to nearly planar geometries (within less than 1°). At such levels, the energy difference between these practically planar and fully planar (C_{2h}) structures is very small (of the order of 0.03−0.06 kcal mol^{-1}). Importantly, the (roto)-vibronic fine structure seen in site-selective fluorescence spectra in ultracold molecular beams[19,76,77] suggests that in its ground state structure, *trans*-stilbene is unequivocally planar. The planarity of *trans*-stilbene at the absolute zero of temperatures has been ultimately confirmed on the theoretical side, by a geometry optimization at the MP2/aug-cc-pVDZ level and a focal point analysis[56] of MP2 and MP3 calculations using extremely large correlation consistent basis sets, along with benchmark CCSD and CCSD(T) calculations using the cc-pVDZ basis set.

For *cis*-stilbene, on the other hand, a distortion from planarity is clearly needed to release enhanced steric strains between the phenyl rings. At the MM3 level, the energy minimum form of *cis*-stilbene is characterized by a dihedral angle ϕ_s of 32.6°. Obviously, the interaction between the phenyl rings in *cis*-stilbene[78] will strongly influence the amplitude of thermal motions.

Table 2 contains the thermally averaged values for the vinylene single and double bond lengths, and the torsion angles,

TABLE 2: Thermally Averaged Conformational Parameters of Isolated *cis*-Stilbene, *trans*-Stilbene, and PV-*n* in the Gas Phase and Crystalline *trans*-Stilbene at Specific Temperatures As Generated by MD(MM3) Simulations or by Means of MM3 Optimization at 0 K

		bond length (Å)[a]		torsion angle (deg)	
	T (K)	C−C vinylene	C=C vinylene	C−C vinylene	C=C vinylene
cis-stilbene	0	1.4794	1.3510	33	9
	100	1.481	1.352	34	9
	200	1.484	1.352	35	9
	300	1.485	1.353	36	10
	400	1.487	1.354	37	11
	500	1.490	1.355	40	11
	600	1.491	1.356	40	12
trans-stilbene	0	1.4747	1.3555	0	0
	100	1.476	1.356	10	3
	200	1.478	1.356	14	6
	300	1.479	1.356	16	6
	400	1.481	1.357	18	7
	500	1.483	1.358	21	8
	600	1.485	1.358	24	9
trans-stilbene	0	1.4724	1.3541	0	0
crystalline	300	1.478	1.358	5	5
PV-3	0	1.4746 (1.4740)	1.3556 (1.3556)	0	0
	300	1.479	1.356	17	6
PV-4	0	1.4743 (1.4739)	1.3557 (1.3558)	0	0
	300	1.479	1.357	17	6
PV-5	0	1.4743 (1.4739)	1.3557 (1.3558)	0	0
	300	1.479	1.356	16	6
PV-6	0	1.4741 (1.4739)	1.3557 (1.3558)	0	0
	300	1.479	1.357	16	6
PV-7	0	1.4740 (1.4739)	1.3557 (1.3558)	0	0
	300	1.479	1.357	16	6

[a] The values in parentheses at 0 K give the average bond lengths in the oligomer chain.

$\bar{\phi}_s$ and $\bar{\phi}_d$, as generated by the MD simulations for isolated molecules of *trans*- and *cis*-stilbene. At 300 K, compared with 0 and 33° at 0 K, an increase of $\bar{\phi}_s$ by 16 and 3° is seen for *trans*- and *cis*-stilbene, respectively. Obviously, this significant difference can be related to much stronger steric hindrances in the latter case. On the experimental side (gas-phase electron diffraction measurements), *trans*-stilbene is characterized by averaged torsion angles $\bar{\phi}_s$ of 30(±15)° and 32°, at temperatures of 473 and 553 K, respectively.[79] These values are qualitatively in line with the thermally averaged torsion angles found from the MD(MM3) simulations (Table 2) at 400−500 K. Also for *cis*-stilbene, an experimental value of 43° is obtained from gas-phase electron diffraction measurements at 435 K,[80] which is in very close agreement with the average value (41°) found on the theoretical side at the same temperature. For *trans*- and *cis*-stilbene in the vacuum at 300 K, 90% of the extracted structures display a torsion angle ϕ_s ranging from −36 to +36°, and from 11 to 62°, respectively.

Increases by ∼6° and ∼1° are similarly seen for the central double bond torsional angle $\bar{\phi}_d$ of *trans*- and *cis*-stilbene at 300 K, respectively, compared with the situation that prevails at absolute zero. For an isolated molecule of *trans*-stilbene at 300 K, the central double bond torsional angles ϕ_d emerging from the MD(MM3) simulations at 300 K display (Figure 6a) a Gaussian distribution centered around $\bar{\phi}_d = 0°$ and characterized by a full width at half-maximum of ∼20°. Hence, in these conditions, 90% of the extracted structures have torsion angles ϕ_d that, in absolute value, do not exceed 12°. In the same conditions, 90% of the structures extracted from the MD(MM3) runs on *cis*-stilbene have torsion angles ϕ_d ranging from −5 to +22° (Figure 6b).

UV−visible measurements (see, e.g., refs 81 and 82) and theoretical calculations (see, e.g., refs 16, 17, and 72) of the one-photon absorption spectrum of both *trans*- and *cis*-stilbene

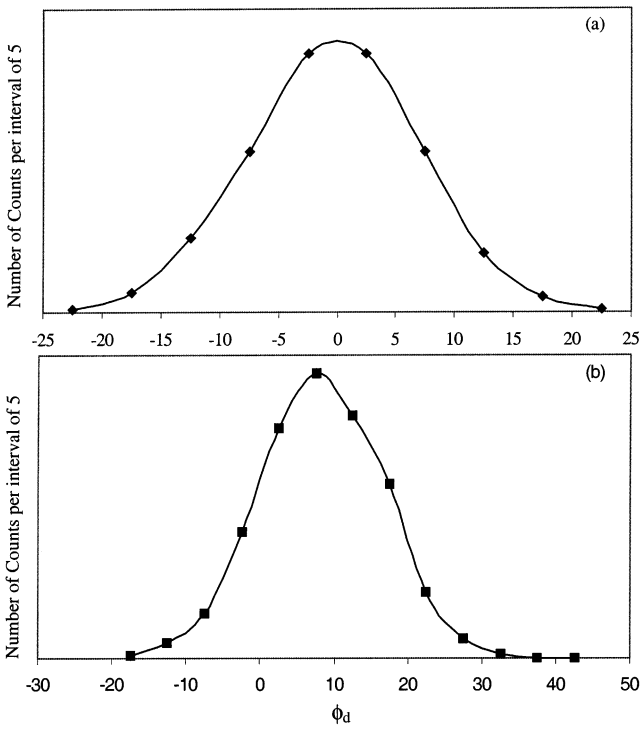

Figure 6. Statistical analysis of the probability distributions of the central double bond torsion angles ϕ_d in (a) *trans*-stilbene and (b) *cis*-stilbene at room temperature in the vacuum.

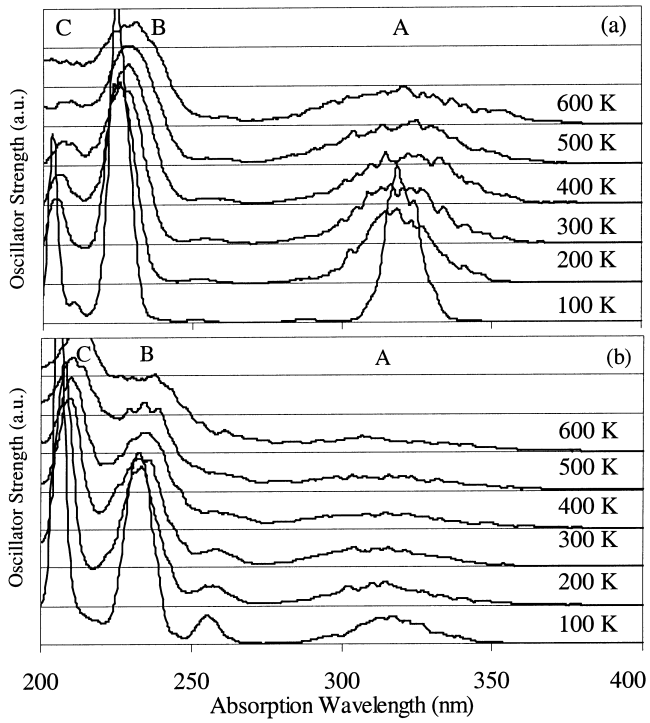

Figure 7. Simulated UV−visible absorption spectra for isolated molecules of (a) *trans*-stilbene and (b) *cis*-stilbene at temperatures ranging from 100 to 600 K with indication of the A, B, and C bands ((Z)INDO/S-CIS//MD(MM3) results).

show three bands, usually labeled A, B, and C, by increasing order of energy. Experimentally, it was found from absorption, fluorescence, and spectral line narrowing measurements, that an increase of temperature induces a blue shift and a broadening of the first absorption band of *trans*-stilbene.[26,83,84] The maxima of the simulated bands in the thermally averaged spectra for both compounds are reported in Table 3 and displayed in Figure 7. Upon analysis of these spectra, it appears that the first absorption band (λ_{max}) is blue shifted for both isomers due to temperature effects, compared with the prediction at 0 K. Interestingly, the shift is much more significant for *cis*-stilbene (8 nm; 0.10 eV) than for *trans*-stilbene (3 nm; 0.04 eV)[54] (300 K).

Compared to the situation that prevails at 0 K, thermal motions at room temperature result in a broadening of the first absorption band of *trans*-stilbene by 23 nm (0.29 eV).[54] Correspondingly, a broadening by 33 nm (0.44 eV) is seen for *cis*-stilbene. At temperatures of 400 K and above, the first two absorption bands clearly overlap (Figure 7) due to enhanced broadening, preventing a straightforward determination of the widths of bands.

For both the trans- and cis-isomers of stilbene, the distribution of lines around λ_{max} is almost symmetric. Previous investigations and analysis of molecular orbital topologies[54] have led to the conclusion that, for *trans*-stilbene, the first absorption energy is strongly influenced by four structural alterations. Because of the nodal structures of the HOMO and LUMO,[18] the value of λ_{max}, which derives directly from the fundamental HOMO−LUMO band gap, is found to be very sensitive to any alteration of the vinylene C−C and C═C bonds, especially the torsion of the vinylene C−C bond, ϕ_s. It has been inferred[18] that, for *trans*-stilbene, the near insensitivity of the thermally averaged value of λ_{max} toward temperature, and the highly symmetric distributions of lines about λ_{max} in the spectra of Figure 7, find their origin in tricky compensations between variations induced for the first excitation energy by various structural distortions, such as the vinylene C−C and C═C bond stretchings, as well as out-of-plane distortions. More specifically, stretchings of the vinylene C−C bond length and the torsion (ϕ_s) around that bond induce in average a blue shift of λ_{max}, whereas the stretching of and the torsion (ϕ_d) around the central vinylene C═C bond have the opposite effect.

For *cis*-stilbene, λ_{max} is found to be sensitive to the same structural alterations (Figure 8). For temperatures ranging from 100 to 600 K, thermally induced stretching and torsion of the vinylene C−C bond yield overall a decrease of λ_{max}, whereas an increase of λ_{max} is on average induced by stretching of the central C═C bond. Compared with *trans*-stilbene, the average impact of the thermally induced stretching of the vinylene single bond is much stronger for the cis-isomer (the slope of the regression line displayed in Figure 8 amounts to −134 nm/Å, to compare with a value of −38 nm/Å for *trans*-stilbene[54]). On the other hand, for the correlation between the stretching of the vinylene double bond and the first vertical excitation energy, the value found for *cis*-stilbene (204 nm/Å) is less than that found for *trans*-stilbene (287 nm/Å).

These striking differences between *trans*- and *cis*-stilbene in the impact on λ_{max} of structural alterations can be easily rationalized from the topologies of the frontier orbitals (HOMO and LUMO, Figure 9). For both isomers, the central vinylene C═C bond relates to bonding and antibonding overlaps of C_{2p} atomic functions in the HOMO and LUMO, respectively, whereas the opposite phase relationships are seen along the vinylene C−C bond. Through destabilization of the HOMO and stabilization of the LUMO, stretching of the vinylene double bond results therefore for both isomers in a red shift of λ_{max} (hence the positive sign of the correlation of Figure 8b, as well as Figure 6c of ref 51). Conversely, stretching of the single C−C vinylene bonds implies a blue shift of λ_{max}, as is apparent from the negative sign of the slope of the correlation displayed in Figure 8a, or Figure 6b of ref 51. For *cis*-stilbene, however,

TABLE 3: Characterization of the Simulated UV-Visible Spectra (ZINDO/S-CIS//MD(MM3) Results[a])

	thermal					thermal and vibronic			
T (K)	*A*[b] (nm)	*A* (eV)	fwhm (nm)	*B* (nm)	*C* (nm)	*A* (nm)	*A* (eV)	fwhm (nm)	exp *A* (eV)
				cis-Stilbene					
0 (^{1}B)	318.7 (0.3668)	3.89	2.00[j]	232.2	204.7				
100	316.3	3.92	23.6	232.6	205.9				
200	311.8	3.98	28.9	233.5	207.7				
300	310.5	3.99	35.3	232.9	209.8				4.48[c]
400	312.0	3.97	52.6	233.8	210.1				
500	309.0	4.01	51.7	234.4	210.7				
600	308.1	4.02	46.1	233.5	213.1				
				trans-Stilbene					
0 (^{1}B$_u$)	322.3 (1.0583)	3.85	2.00[j]	225.4	201.7			6 × 2.00[j,k]	3.71,[d] 4.00[e]
100	320.3	3.87	11.30	223.9	203.5	294.2[l]	4.21[l]	28.91[l]	
200	318.4	3.89	20.99	225.4	204.1	293.9[l]	4.22[l]	32.65[l]	
300	318.9	3.89	25.63	225.7	205.9	295.3	4.20	34.91	3.98,[f] 4.22,[g] 4.0[h]
300	320.2	3.87	21.86						
400	320.6	3.87	28.52	228.4	206.8	296.6	4.18	36.21	
500	317.6	3.90	35.07	228.1	207.5	296.8	4.18	37.52	
600	316.6	3.92	41.56	231.1	207.4	298.0	4.16	39.40	
				trans-Stilbene					
				Crystalline					
300	323.3	3.84	19.83	224.8	204.4	298.2	4.16	33.64	
				PV-3					
0 (^{1}B$_u$)	364.4 (1.8296)	3.40	2.00[j]	227.6	201.6				
300	359.4	3.45	26.24	228.6	207.3	332.9	3.72	40.75	3.44[i]
300	358.6	3.46	23.97						
				PV-4					
0 (^{1}B$_u$)	386.6 (2.25510)	3.21	2.00[j]	227.4	201.6				
300	379.5	3.27	26.78	228.6	207.9	350.2	3.54	43.92	3.20[i]
300	378.5	3.28	24.35						
				PV-5					
0 (^{1}B$_u$)	398.1 (3.2822)	3.11	2.00[j]	226.2	201.0				
300	389.9	3.18	23.17			359.3	3.45	44.00	3.08[i]
				PV-6					
0 (π) (^{1}B$_u$)	405.8 (4.0095)	3.06	2.00[j]						
300	395.5	3.13	24.76			365.4	3.39	45.45	3.01[i]
				PV-7					
0 (π) (^{1}B$_u$)	410.8 (4.7410)	3.02	2.00[j]						
300	400.8	3.09	23.96			370.1	3.35	45.50	2.97[i]
				PPV					
0	449.4[m]	2.76[m]				401.0[m]	3.09[m]		

[a] Values in italic are the results of (Z)INDO/S-CIS calculations with an active space restricted to π and π^* orbitals which are corrected using eq 1. [b] Values in parentheses are oscillator strengths in au. [c] One-photon absorption spectrum in ethanol at room temperature [Beale, R. N.; Roe, E. M. F. *J. Chem. Soc.* **1953**, 2755]. [d] 0−0 line resolved in dibenzyl crystals at 20 K [Dyck, R. H.; McClure, D. S. *J. Chem. Phys.* **1962**, *36*, 2326]. [e] 0−0 transition observed in molecular beams [Champagne B. B.; et al. *J. Phys. Chem.* **1990**, *94*, 6]. [f] One-photon absorption spectrum in benzene at room temperature [Suzuki, H. *Bull. Chem. Jpn.* **1960**, *33*, 379]. [g] One-photon absorption spectrum in *n*-heptane at room temperature [Suzuki, H. *Bull. Chem. Jpn.* **1960**, *33*, 379]. [h] One-photon absorption spectrum in 3-methylpentane at room temperature [Hohlneicher, G.; Dick, B. *J. Photochem.* **1984**, *27*, 215]. [i] One-photon absorption spectrum in THF at room temperature [Schenk, R.; Gregorius, H.; Müllen, K. *Adv. Mater.* **1995**, *3*, 492]. [j] Chosen fwhm value for convoluting each individual line in the spike spectra. [k] Six vibronic transitions are retained in the computation. [l] Low correlation due to description of multiple bands with a single Gaussian function; however, visual inspection of Figure 8a supports the suggested maximum and broadening. [m] Extrapolated values; see Figure 2.

additional antibonding and bonding through-space interactions between the closer phenyl rings help to further stabilize the HOMO and destabilize the LUMO, respectively, upon stretching of the vinylene single bond. This explains the much stronger impact of this structural alteration on λ_{max}, compared to the trans-isomer. On the other hand, the alteration of through-space interactions between the phenyl rings upon stretching of the central C═C vinylene bond tends to compensate the direct outcomes of the overlaps of the C_{2p} atomic functions describing that bond. Indeed, if tight-binding effects imply a destabilization of the HOMO and a stabilization of the LUMO, the appeasement of through-space interactions between the phenyl rings lead conversely to a stabilization of the HOMO, and a destabilization of the LUMO. Hence, the smaller impact of the stretching of the central double bond of the cis-isomer on λ_{max}, compared with *trans*-stilbene. Also, due to these through-space interactions between phenyl rings, a significant reduction is seen for *cis*-stilbene in the influence on λ_{max} of the torsions, ϕ_s and ϕ_d, of the single and central double bonds, respectively.

For both compounds, the remaining two bands in the calculated spectra exhibit less pronounced broadenings and minor red shifts of about 1 nm (0.02 eV; B band) and 5 nm (0.14 eV; C band), due to temperature effects at 300 K (Table 3). Two additional weak bands at about 260 nm (4.77 eV) and 280 nm (4.43 eV) can be seen in the absorption spectra of *trans*-stilbene (Figure 7a) at nonzero temperatures, which relate to the weak (HOMO → LUMO+1) ^1B_u and the symmetry forbidden (HOMO → LUMO+3) ^1A_g transitions, respectively. The latter gains intensity because of symmetry lowering due to thermal distortions. The related transitions are allowed by the

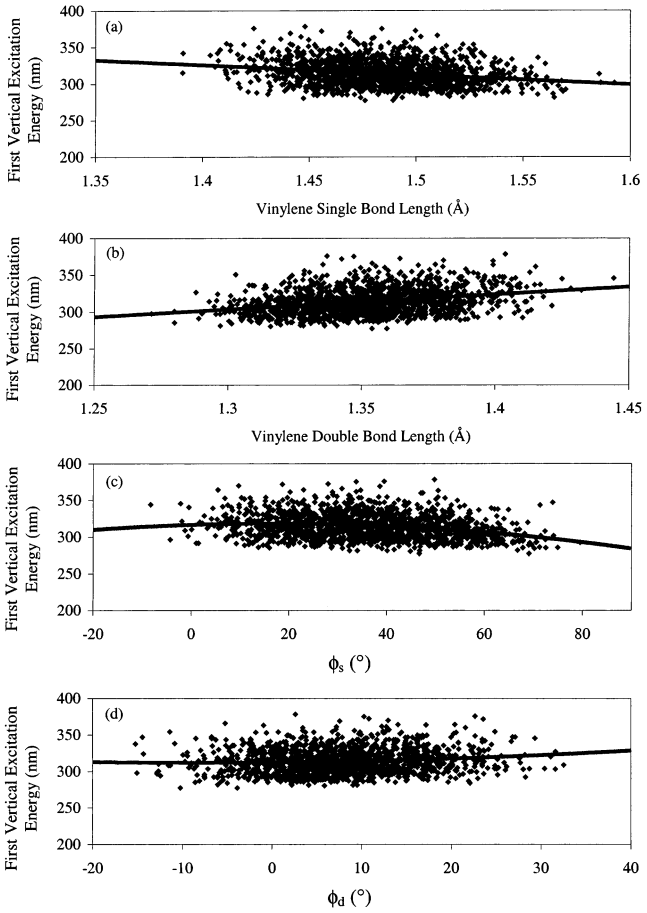

Figure 8. Statistical correlation at room temperature between the first excitation energy, λ_{max} of *cis*-stilbene, and the vinylene (a) single bond length (regression given by $y = -133.75x + 512.88$), (b) double bond length ($y = 204.1x + 38.148$), (c) single bond torsion angle, ϕ_s ($y = -0.0064x^2 + 0.2105x + 316.55$), and (d) double bond torsion angle, ϕ_d ($y = 0.0071x^2 + 0.12x + 312.48$) ((Z)INDO/S-CIS//MD-(MM3) results at 300 K).

C_2 symmetry of the 0 K structure of *cis*-stilbene and are found at about 290 nm (4.28 eV) and 255 nm (4.86 eV).

Isolated PV-*n* Chains. Most of the observations reported so far for an isolated *trans*-stilbene molecule (or PV-2) straightforwardly apply for larger PV-*n* oligomer chains. The MM3 optimizations indicate that the outmost vinylene C−C and C═C bond lengths of larger systems are comparable to those found for PV-2, whereas the inner parts of the oligomers (given in parentheses in Table 2) exhibit reduced bond length alternations in the energy minimum form. These differences in bond lengths are typical of termination effects. With MM3, the inner bond lengths are reproduced within 0.01 Å accuracy, in comparison with calculations using bond alternation potentials parametrized on DFT results using the LDA (local density approximation) functional.[85] All structural parameters are converged from PV-6 and beyond, indicating saturation to the polymer regime. The differences between inner and outer bond lengths is blurred out by thermal effects already at 100 K, making such distinction irrelevant in practical situations. The thermally averaged value for the torsion angle ϕ_s, describing the out-of-plane rotation of the phenyl rings, is nearly constant for all investigated oligomers, PV-*n*, and amounts to 16° at 300 K. Similarly, the average torsion of the vinylene double bonds is independent of system size (6° at room temperature).

Figure 2a shows that the lowest energy absorption peak gets red shifted with increasing chain length, in agreement with various theoretical and experimental studies (see e.g. refs 29, 35, 72). Extrapolation of λ_{max} against $1/n$ at 0 K leads to an estimate of the vertical absorption threshold of PPV at an energy of 2.76 eV (or 449 nm). The main characteristics of the simulated UV−visible absorption spectra at a temperature of 300 K (Figure 10) are quantified in Table 3. It can be seen that, at constant temperature, the amplitude of the thermally induced blue shift of the first absorption band increases with increasing system size (PV-2 3 nm, 0.04 eV; PV-3 5 nm, 0.05 eV; PV-4 7 nm, 0.06 eV; PV-5 8 nm, 0.07 eV; PV-6 10 nm, 0.07 eV; PV-7 10 nm, 0.07 eV). For *trans*-stilbene and the smallest PV-*n* chains ($n = 2-4$), the first absorption band undergoes simultaneously a constant broadening, which at room temperature amounts to about 24 nm (0.29 eV for *trans*-stilbene and 0.20 eV for larger PV oligomers, taking into account the width, 2 nm or 0.02 eV, of the spread function). Notice that, for PV-*n* chains larger than PV-4, the restriction of the active space to π levels only results in a limitation of the thermal broadening of band A estimated to ∼2 nm (0.05 eV for *trans*-stilbene and 0.02 eV for larger oligomers), at room temperature; hence the best estimate for thermal broadening amounts also in this case to ∼24 nm (0.20 eV).

Various thermally averaged vibronic sequences at temperatures ranging from 0 to 600 K are displayed for *trans*-stilbene in Figure 11a to evaluate the cumulated effects of the thermal and vibronic broadenings. According to these simulations, the vibronic fine structure must be clearly apparent in the gas phase at low temperatures (100 and 200 K) but must disappear in a single band of about 35 nm (0.50 eV) width at 300 K (Table 3). Taking into account the width of the spread function, this implies a combined broadening of 33 nm (0.48 eV; compared to a broadening of 24 nm (0.20 eV) when only temperature effects are accounted for). Notice that the apparent impact of the vibronic broadening on bandwidths becomes much less apparent at higher temperature (Table 3). Thermal broadening and vibronic coupling yield overall a global blue shift of the first absorption band of *trans*-stilbene by 27 nm (0.35 eV) at room temperature, compared to the 0 K value of 322.3 nm (3.86 eV). Similarly, for the other PPV oligomers, vibronic fine structures can no longer be resolved at room temperature (Figure 11b). In this case, the cumulated impact of thermal and vibronic broadenings increases with system size and tends to converge to about 46 nm (0.41 eV) (taking account of the impact of the restriction of the active space to π-orbitals and of the width of the employed spread function). Upon extrapolation to the polymer limit, the maximum of the thermally and vibronically broadened first absorption band of PPV (λ_{max}) lies at about 401.0 nm (3.09 eV), which implies a blue shift by nearly 50 nm (0.33 eV) compared to the 0 K value.

***trans*-Stilbene in Crystalline Phase.** Upon inspection of the thermally averaged geometry parameters reported in Table 2, it immediately appears that intermolecular interactions at room temperature in the crystal have very limited effects on bond lengths (0.001−0.002 Å) or on the torsion of the vinylene double bond, as described by the ϕ_d dihedral angle (about 1° difference), compared to the situation that prevails in a vacuum. On the other hand, packing effects and intermolecular forces strongly impede rotations of the phenyl groups about the vinylene single bonds. Unsurprisingly, the thermally averaged value of ϕ_s at room temperature decreases by 11°, compared with the case of an isolated molecule. This difference is even more striking when one compares the largest values found at room temperature for ϕ_s, 67° and only 26°, from the MD(MM3′) simulations on an isolated molecule and on the model crystalline cluster, respec-

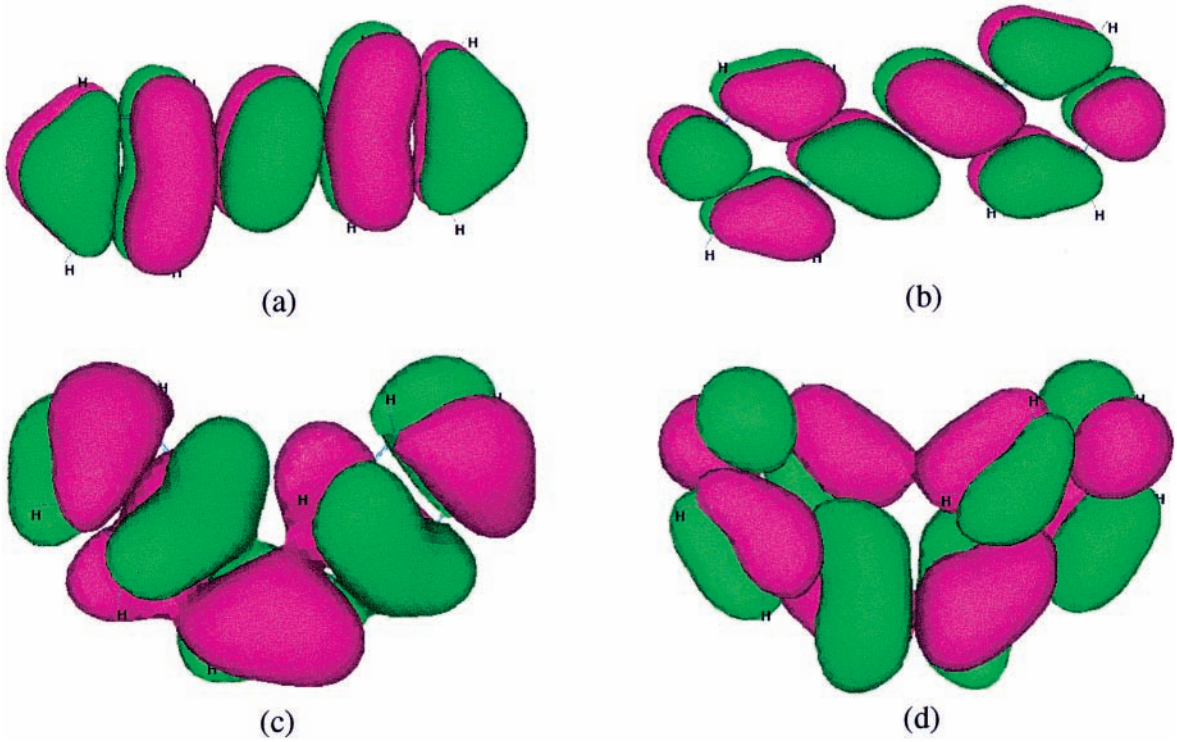

Figure 9. Molecular orbital contours to account for the restriction of the active space to π and π^* orbitals. (a) HOMO and (b) LUMO of *trans*-stilbene; (c) HOMO and (d) LUMO of *cis*-stilbene ((Z)INDO/S-CIS//MM3 results).

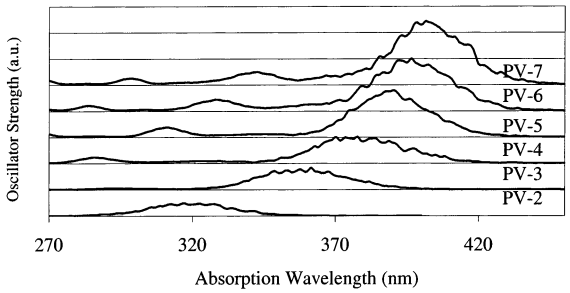

Figure 10. Thermally averaged UV−visible absorption spectra of all isolated PV-*n* oligomers in the gas phase and at room temperature ((Z)-INDO/S-CIS//MD(MM3) results). (The spectra for PV-5 to PV-7 are shifted by 26.226 nm to account for the restriction of the active space to π and π^* orbitals.)

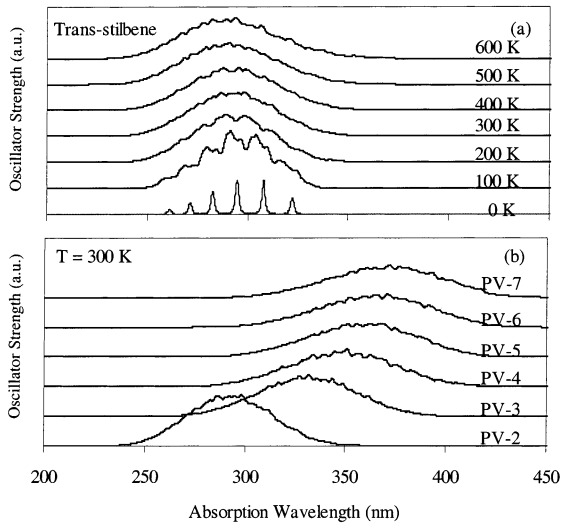

Figure 11. (a) Simulation absorption spectra for the vibronic progressions of all λ_{max} values from the previous coupled (Z)INDO/S-CIS//MD(MM3) calculations for *trans*-stilbene in the gas phase at different temperatures. (b) Simulated vibronic absorption spectra for the PV oligomers at room temperature (from previous (Z)INDO/S-CIS//MD-(MM3) results). (The spectra for PV-5 to PV-7 are shifted by 26.226 nm to account for the limitation of the π active space.)

tively. Interestingly, the value calculated upon thermal averaging for the ϕ_s dihedral angle (5°) is in excellent agreement with the structures inferred from XRD studies, which also point out a value of ∼5°.[37,38,62]

Figure 12 compares the simulated UV−visible absorption spectra of *trans*-stilbene at room temperature in the gas phase (lower spectrum) and in a crystalline matrix (upper spectrum). Hindrances of thermal out-of-plane distortions due to packing effects slightly affect the shape and position of the first absorption band (A), without leading to significant changes of the integrated intensity. All other bands are found to be almost unaffected by such effects. Compared with what was found for an isolated molecule (Table 3), a red shift by 4 nm (0.05 eV) is seen for λ_{max} at room temperature, whereas the width of the first absorption band decreases by almost 6 nm (0.07 eV). When vibronic broadening at room temperature (Table 3) is included, and the bandwidth of the spread function is subtracted, the total broadening amounts to a fwhm parameter of 32 (=34−2) nm (0.42 eV), to compare with a value of 33 (=35−2) nm (0.45 eV) for the isolated molecule.

On the basis of the correlations presented previously[18] for an isolated molecule of *trans*-stilbene, the limitation of the thermally averaged value of ϕ_s should lead to a red shift by 9 nm (0.11 eV) at room temperature. Other factors must therefore be considered to explain why a red shift of only 4 nm (0.05 eV) occurs for *trans*-stilbene in the crystal phase. From the statistical correlations displayed in Figure 13, it appears that the stretching of the vinylene C−C bond has a much stronger effect on the position of λ_{max} in the crystal than in the vacuum (the average linear correlation with the excitation energy shows a slope of −173 Å/nm, to compare with a slope of −38 Å/nm for isolated *trans*-stilbene). This enhanced average dependence

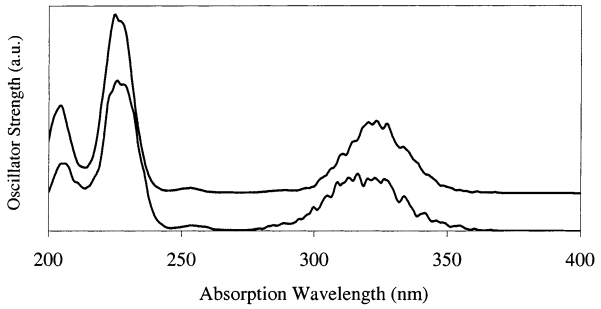

Figure 12. Comparison of the spectra for *trans*-stilbene in the gas (lower) and in crystal (upper spectrum) phases ((Z)INDO/S-CIS//MD-(MM3) results at 300 K).

of the first excitation energy on the vinylene C−C bond length therefore partially compensates the red shift arising because of the limitations of the amplitude of out-of-plane distortions and reflects stronger couplings between various intramolecular structural distortions, due to steric hindrances with the surrounding crystalline matrix.

Conclusions

The issue of band broadening is of particular relevance for standard conjugated polymer materials such as poly(*p*-phenylene vinylene) (PPV), because a striking and common feature of their optical spectrum is the exceedingly large width (150 nm or more) of the first absorption band, due to alterations of the conjugation length by inherent structural defects in the polymer matrix.[25] Formally, deconvolution of this band into individual contributions for finite PV-*n* oligomer chains should in principle deliver straightforward and quantitative information on the relative abundances in the material of conjugated segments with varying length. In practice, such an analysis is extremely challenging, owing to the many factors that can contribute to band broadening. Among these, thermal dynamic disorder is certainly the one that so far received the less attention.

In sharp contrast with so many studies of excited states, which to the greatest extent focus on accurate determinations of excitation energies and transition moments for individual molecular structures allegedly taken in their ground-state energy

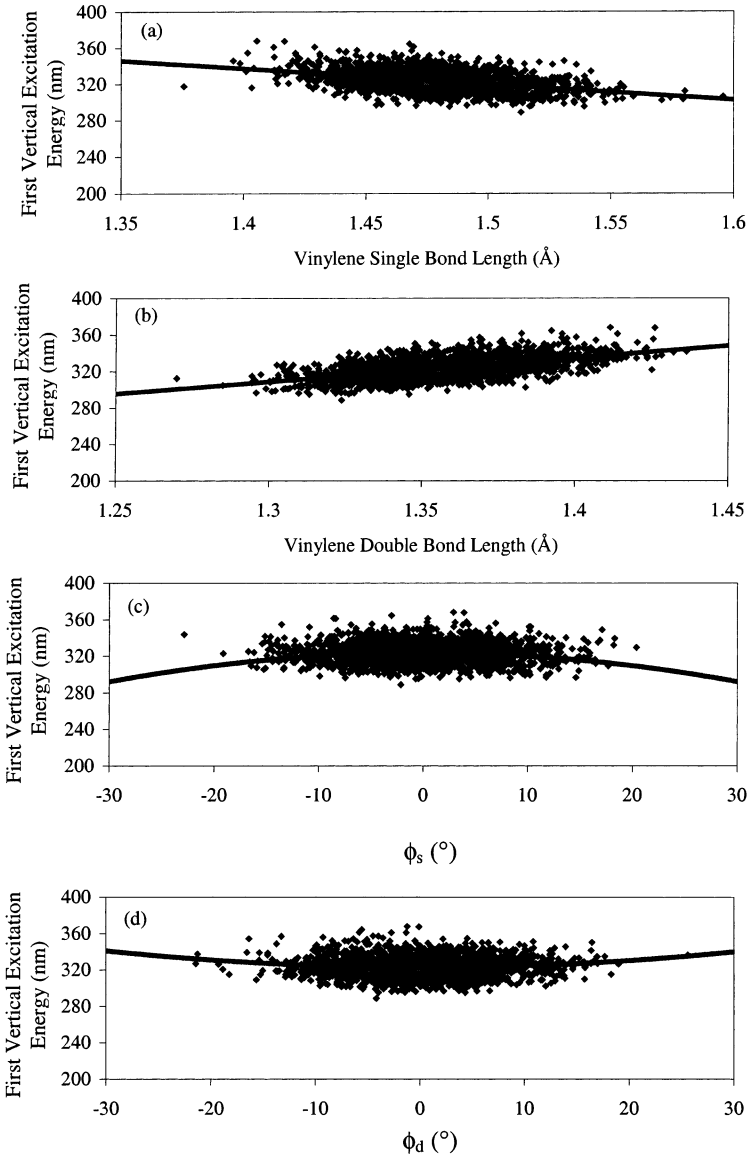

Figure 13. Statistical correlation at room temperature between the first excitation energy, λ_{max} of *trans*-stilbene in the crystalline phase, and the vinylene (a) single bond length (regression given by $y = -173x + 579.34$), (b) double bond length ($y = 261.77x - 31.687$), (c) single bond torsion angle, ϕ_s ($y = -0.004x^2 - 0.0227x + 323.71$), and (d) double bond torsion angle, ϕ_d ($y = 0.0196x^2 - 0.016x + 322.83$) ((Z)INDO/S-CIS//MD-(MM3) results at 300 K).

minimum forms, this work aims at providing consistent insights into the shifts and band broadenings induced by temperature effects in the UV−visible absorption spectra of PV-*n* oligomers converging to PPV. In this purpose, (Z)INDO/S-CIS calculations have been carried out on various and large sets of thermally distorted structures, generated along molecular dynamic trajectories on potential energy surfaces described by a classical (MM3) molecular mechanics force field. Significant band broadenings and blue shifts (up to 10 nm, or 0.07 eV, for PV-7, at 300 K) are seen for the first absorption band, because of thermal motions. For the first absorption band of *trans*-stilbene and related PV-*n* chains, thermal broadening in the gas phase amounts to 11 nm (0.14 eV) and ∼24 nm (0.29 eV for *trans*-stilbene and 0.20 eV for larger oligomers) at 100 and 300 K, respectively. Thermal broadening strongly intensifies for the first absorption band of *cis*-stilbene (33 nm, or 0.44 eV at 298 K), owing to stronger steric hindrances and through-space interactions between the phenyl rings. Compared with *trans*-stilbene, a stronger band shift is also noticed for *cis*-stilbene (8 nm, or 0.10 eV versus 3 nm, or 0.04 eV, at 298 K). As a bonus, the MD(MM3) calculations, presented in this study, enables consistent insights into the average gas-phase structures of *cis*- and *trans*-stilbene at different temperatures.

Upon an extension of this study on a model crystalline cluster of *trans*-stilbene, it appears that compared with the situation that prevails in the vacuum, the impact of intermolecular interactions and packing effects in the solid phase on the thermal broadening of bands leads to a limitation of the width of the band by 6 nm (0.07 eV) only. Hence a constant thermal width of 18 nm (0.19 eV) can be inferred for the first absorption band of *trans*-stilbene in the solid phase, which is perfectly in line with the commonly used value of 20 nm (for measurements at room temperature).

Very significant also is the outcome of vibronic couplings on bandwidths, which is found to be of the same order of magnitude as that induced by temperature effects. In straightforward analogy with the work of ref 35, the vibronic sequences that have been incorporated into the (Z)INDO/S-CIS//MD-(MM3) model have been computed by using fitted Huang−Rhys factors and a single effective vibrational mode for the first excited state. It is shown on theoretical grounds that at room temperature vibronic sequences can no longer be apparent in the absorption spectrum. When both thermal and vibronic broadening are accounted for, the width of the first absorption band of PV-*n* chains ranges at 300 K from 33 nm (0.48 eV, $n = 2$) to 46 nm (0.41 eV, $n = 7$). With regard to these results and the computed excitation spectra, it can be therefore safely concluded that the optical spectrum presented in ref 72 for a PPV sample actually relates to a polymer material that incorporates a very significant proportion of planar segments of very limited conjugation length, comparable to that of the PV-2, PV-3, and PV-4 chains.

Acknowledgment. We acknowledge financial support from the Bijzonder Onderzoeksfonds (BOF) of the LUC, within the framework of a multidisciplinary project on Conjugated Polymers for Polymer Electronics (COPPEC), and from the Fonds voor Wetenschappelijk Onderzoek-Vlaanderen (FWO). We are grateful to Profs. D. Vanderzande and J. Gelan (Group of Organic Chemistry, LUC, Belgium) for support and interesting discussions.

References and Notes

(1) Shirakawa, H.; Louis, E. J.; MacDiarmid, A. G.; Chiang, C. K.; Heeger A. J. *J. Chem. Soc., Chem. Commun.* **1977**, 579.

(2) André, J. M.; Delhalle, J.; Brédas, J. L. *Quantum Chemistry Aided Design of Organic Polymers − An Introduction to the Quantum Chemistry of Organic Polymers and Its Applications*; World Scientific Publishing Co. Pte. Ltd.: London, 1991.

(3) Heeger, A. J., Ed. *Proceedings of the International Conference on Science and Technology of Synthetic Metal*; Synthetic Metals; Elsevier: Amsterdam, 1995; p 69.

(4) Wegner, G.; Müllen, K. *Electronic Materials: The Oligomer Approach*; Wiley-VCH: Weinheim, 1998.

(5) Friend, R. H.; Gymer, R. W.; Holmes, A. B.; Burroughes, J. H.; Marks, R. N.; Taliani, C.; Bradley, D. D. C.; Dos Santos, D. A.; Brédas, J. L.; Lögdlund, M.; Salaneck, W. R. *Nature* **1999**, *397*, 121.

(6) Clery, D. *Science* **1994**, *263*, 1700.

(7) Monk, P.; Mortimer, R. J.; Rosseinsky, D. R. *Electrochromism: Fundamentals and Applications*; VCH: Weinheim, 1995.

(8) Brown, A. R.; Jarrett, C. P.; De Leeuw, D.; Matters, M. *Synth. Met.* **1997**, *8*, 37.

(9) Horowitz, G. *Adv. Mater.* **1998**, *10*, 365.

(10) Heywang, G. J. *Adv. Mater.* **1992**, *4*, 116.

(11) Sariciftci, N. S.; Smilowitz, L.; Heeger, A. J.; Wundl, F. *Science* **1992**, *258*, 1474.

(12) Stoes, E.; Vangeneugden, D.; Nagels, L. J.; Vanderzande, D.; Gelan, J. *Electroanalysis* **1999**, *11*, 65.

(13) Reynolds, J. R. *Chemtech* **1990**, *18*, 440.

(14) Burroughes, J. H.; Bradley, D. D. C.; Brown, A. R.; Marks, R. N.; Mackay, K.; Friend, R. H.; Burns, P. L.; Holmes, A. B. *Nature* **1990**, *347*, 539.

(15) Johansson, N.; Cacialli, F.; Xing, K. Z.; Beamson, G.; Clark, D. T.; Friend, R. H.; Salaneck, W. R. *Synth. Met.* **1998**, *92*, 207.

(16) Molina, V.; Merchàn, M.; Roos, B. O. *J. Phys. Chem. A* **1997**, *101*, 3478.

(17) Molina, V.; Merchàn, M.; Roos, B. O. *Spectrochim. Acta A* **1999**, *55*, 433.

(18) Kwasniewski, S. P.; Deleuze, M. S.; François, J. P. *Int. J. Quantum Chem.* **2000**, *80*, 672.

(19) Waldeck, D. H. *Chem. Rev.* **1991**, *91*, 415.

(20) Mohrschaldt, R.; Schroeder, J.; Schwarzer, D.; Troe, J.; Vöhringer, P. *J. Chem. Phys.* **1994**, *101*, 7566.

(21) Mitchell, A. C. G.; Zemansky, M. W. *Resonance radiation and excited atoms*; Cambridge University Press: Cambridge, U.K., 1971.

(22) Peeters, E.; Ramos, A. M.; Meskers, S. C. J.; Janssen, R. A. J. *J. Chem. Phys.* **2000**, *112*, 9445.

(23) Heeger, A. J.; Kivelson, S.; Schrieffer, J. R.; Su, W. P. *Rev. Mod. Phys.* **1988**, *60*, 781.

(24) Baeriswyl, D.; Campbell, D. K.; Mazumdar, S. *Springer Series in Solid State Sciences 102*; Kiess, H. G., Ed.; Springer: Berlin, 1992.

(25) Scholes, G. D.; Larsen, D. S.; Fleming, G. R.; Rumbles, G.; Burn, P. L. *Phys. Rev. B* **2000**, *61*, 13670.

(26) Heun, S.; Mahrt, R. F.; Greiner, A.; Lemmer, U.; Bässler, H.; Halliday, D. A.; Bradley, D. D. C.; Burn, P. L.; Holmes, A. B. *J. Phys. Condens. Matter* **1993**, *5*, 247.

(27) Pilcher, K.; Halliday, D. A.; Bradley, D. D. C.; Burn, P. L.; Friend, R. H.; Holmes, A. B. *J. Phys. Condens. Matter* **1993**, *5*, 7155.

(28) Tian, B.; Zerbi, G.; Müllen, K. *J. Chem. Phys.* **1991**, *95*, 3198.

(29) Woo, H. S.; Lhost, O.; Graham, S. C.; Bradley, D. D. C.; Friend, R. H.; Quattrocchi, C.; Brédas, J. L.; Schenk, R.; Müllen, K. *Synth. Met.* **1993**, *59*, 13.

(30) Hagler, T. W.; Pakbaz, K.; Voss, K. F.; Heeger, A. J. *Phys. Rev. B* **1991**, *44*, 8652.

(31) Rauscher, U.; Schültz, L.; Greiner, A.; Bässler, H. *J. Phys. Condens. Matter* **1989**, *1*, 9751.

(32) Lhost, O.; Brédas, J. L. *J. Chem. Phys.* **1992**, *96*, 5279.

(33) Cornil, J.; Beljonne, D.; Calbert, J.-P.; Brédas, J.-L. *Adv. Mater.* **2001**, *13*, 1053.

(34) Yu, J.; Fann, W. S.; Lin, S. H. *Theor. Chem. Acc.* **2000**, *103*, 374.

(35) Cornil, J.; Beljonne, D.; Shuai, Z.; Hagler, T. W.; Campbell, I.; Bradley, D. D. C.; Brédas, J. L.; Spangler, C. W.; Müllen, K. *Chem. Phys. Lett.* **1995**, *247*, 425.

(36) Harada, J.; Ogawa, K. *J. Am. Chem. Soc.* **2001**, *123*, 10884.

(37) Finder, C. J.; Newton, M. G.; Allinger, N. L. *Acta Crystallogr.* **1974**, *B30*, 411.

(38) Bouwstra, J. A.; Schouten, A.; Kroon, J. *Acta Crystallogr.* **1984**, *C40*, 428.

(39) Ogawa, K.; Sano, T.; Yoshimura, S.; Takeuchi, Y.; Toriumi, K. *J. Am. Chem. Soc.* **1992**, *114*, 1041.

(40) Allinger, N. L.; Burkert, U. *Molecular Mechanics*; American Chemical Society: Washington, DC, 1982.

(41) Haile, J. M. *Molecular Dynamics Simulation*; John Wiley & Sons: New York, 1997.

(42) Claes, L.; François, J. P.; Deleuze, M. S. *Chem. Phys. Lett.* **2001**, *339*, 216.

(43) Warshel, A.; Levitt, M. *J. Mol. Biol.* **1976**, *103*, 227.

(44) Coutinho, K.; Canuto, S.; Zerner, M. C. *J. Chem. Phys.* **2000**, *122*, 9874.

(45) Roitberg, A. E.; Worthington, S. E.; Holden, M. J.; Mayhew, M. P.; Krauss, M. *J. Am. Chem. Soc.* **2000**, *122*, 7312.

(46) Allinger, N. L.; Yu, Y. H.; Lii, J. H. *J. Am. Chem. Soc.* **1989**, *111*, 8551.

(47) Lii, J. H.; Allinger, N. L. *J. Am. Chem. Soc.* **1989**, *111*, 8566.

(48) Lii, J. H.; Allinger, N. L. *J. Am. Chem. Soc.* **1989**, *111*, 8576.

(49) Kao, J.; Allinger, N. L. *J. Am. Chem. Soc.* **1977**, *99*, 975.

(50) Kao, J. *J. Am. Chem. Soc.* **1987**, *109*, 3817.

(51) Nevins, N.; Lii, J.-H.; Allinger, N. L. *J. Comput. Chem.* **1996**, *17*, 695.

(52) Gundertofte, K.; Liljefors, T.; Norrby, P.-o.; Petterson, I. *J. Comput. Chem.* **1998**, *17*, 429.

(53) Gonzalez, C.; Lim, E. C. *J. Phys. Chem. A* **2000**, *104*, 2953.

(54) Kwasniewski, S. P.; François, J. P.; Deleuze, M. S. *Int. J. Quantum Chem.* **2001**, *85*, 557.

(55) Galli, S.; Mercandelli, P.; Sironi, A. *J. Am. Chem. Soc.* **1999**, *121*, 3767.

(56) Kwasniewski, S. P.; François, J. P.; Deleuze, M. S. Accepted for publication in *J. Chem. Phys.* **2003**, *118*, 7823.

(57) Deleuze, M.; Zerbetto, F.; Leigh, D. A. *J. Am. Chem. Soc.* **1999**, *121*, 2364.

(58) Deleuze, M.; Zerbetto, F. *J. Am. Chem. Soc.* **1999**, *121*, 5281.

(59) Ponder, J. W. *Tinker 3.1, Software Tools for Molecular Design*, 1996.

(60) Berendsen, H. J. C.; Postma, J. P. M.; van Gunsteren, W. F.; DiNola, A.; Haak, J. R. *J. Chem. Phys.* **1984**, *81*, 3684.

(61) Beeman, D. *J. Comput. Phys.* **1976**, *20*, 130.

(62) Hoekstra, A.; Meertens, P.; Vos, A. *Acta Crystallogr.* **1975**, *B31*, 2813.

(63) Zerner, M. C.; Loew, G. H.; Kirchner, R. F.; Mueller-Westerhoff, U. T. *J. Am. Chem. Soc.* **1980**, *102*, 589.

(64) Pearl, G. M.; Zerner, M. C.; Broo, A. McKelvey, J. *J. Comput. Chem.* **1998**, *19*, 781.

(65) Zerner, M. C.; Ridley, J. E.; Bacon, A. D.; Edwards, W. D.; Head, J. D.; McKelvey, J.; Culberson, J. C.; Knappe, P.; Cory, M. G.; Weiner, B.; Baker, J. D.; Parkinson, W. A.; Kannis, D.; Yu, J.; Roesch, N.; Kotzian, M.; Tamm, T.; Karelson, M. M.; Zheng, X.; Pearl, G.; Broo, A.; Albert, K.; Cullen, J. M.; Cramer, C. J.; Truhlar, D. G.; Li, J.; Hawkins G. D.; Liotard, D. A.; *ZINDO − A semiempirical program package*, University of Florida: Gainesville, FL, 1996.

(66) Bauernschmitt, R.; Ahlrichs, R. *Chem. Phys. Lett.* **1996**, *256*, 454.

(67) Casida, M. E.; Jamorski, C.; Casida, K. C.; Salahub, D. R. *J. Chem. Phys.* **1998**, *108*, 4439.

(68) Stratmann, R. E.; Scuseria, G. E.; Frisch, M. J. *J. Chem. Phys.* **1998**, *109*, 8218.

(69) Andersson, K.; Malmqvist, P.-Å; Roos, B. O. *J. Chem. Phys.* **1992**, *96*, 1218.

(70) In this scheme, the INDO/1 [Pople, J. A.; Beveridge, D. L.; Dobosh, P. A. *J. Chem. Phys.* **1967**, *47*, 2026] method is used in combination with the CIS [Foresman, J. B.; Head-Gordon, M.; Pople, J. A.; Frisch, M. J. *J. Phys. Chem.* **1992**, *96*, 135] scheme, to partially account for dynamic electron correlation. Use is made of the spectroscopic Mataga−Nishimoto parametrization [Mataga, N.; Nishimoto, K. *Z. Chem. Phys.* **1957**, *13*, 140], which best reproduces experimental absorption spectra within the (Z)INDO/S-CIS formalism. Notice that (Z)INDO/S-CIS has been parametrized to correctly reproduce the peak position of bands (which does not necessarily coincide with the energy location of the 0−0 vibronic transition). With the (Z)INDO/S-CIS scheme, oscillator strengths are calculated for vertical electron transitions using the dipole approximation.

(71) Cornil, J.; Beljonne, D.; Brédas J. L. *J. Chem. Phys.* **1995**, *103*, 834.

(72) Obrzut, J.; Karasz, F. E. *J. Chem. Phys.* **1987**, *87*, 2349.

(73) (a) Fischer, G. *Vibronic Coupling: The Interaction between the Electronic and Nuclear Motions*: Academic Press: London, 1984. (b) J. Gierschner, H.-G. Mack, L. Lüer, D. Oelkrug *J. Chem. Phys.* **2002**, *116*, 8596.

(74) Galvao, D. S.; Soos, Z. G.; Ramasesha, S.; Etemad, S. *J. Chem. Phys.* **1993**, *98*, 3016.

(75) Choi, C. H.; Kertesz, M. *J. Phys. Chem. A* **1997**, *101*, 3823.

(76) Champagne, B. B.; Pfanstiel, J. F.; Plusquellic, D. F.; Pratt, D. W.; van Herpen, W. M.; Meerts, W. L. *J. Phys. Chem.* **1990**, *94*, 6.

(77) Chiang, W.-Y.; Laane, J. *J. Chem. Phys.* **1994**, *100*, 8755.

(78) Bearpark, M. J.; Bernardi, F.; Clifford, S.; Olivucci, M.; Robb, M. A.; Vreven, T. *J. Phys. Chem. A* **1997**, *101*, 3841.

(79) Traetteberg, M.; Frantsen, E. B.; Mijlhoff, F. C.; Hoekstra, A. *J. Mol. Struct.* **1975**, *26*, 57.

(80) Traetteberg, M.; Frantsen, E. B. *J. Mol. Struct.* **1975**, *26*, 69.

(81) Beale, R. N.; Roe, E. M. F. *J. Chem. Soc.* **1953**, 2755.

(82) Hohlneicher, G.; Dick, B. *J. Photochem.* **1984**, *27*, 215.

(83) Sheridan, A. K.; Lupton, J. M.; Samuel, I. D. W.; Bradley, D. D. C. *Chem. Phys. Lett.* **2000**, *322*, 51.

(84) Spiegelberg, C.; Peyghambarian, N.; Kippelen, B. *Appl. Phys. Lett.* **1999**, *75*, 748.

(85) Förner, W.; Bogar, F.; Knab, R. *J. Mol. Struct. (THEOCHEM)* **1998**, *430*, 73.